

Space weathering and aging effects observed on geostationary satellites

Bezovec 2023 - Conference of Young Astronomers
June 17th 2023



Name:

Mgr. Matej Zigo

FMPI Supervisor:

doc. RNDr. Leonard Kornoš, PhD.

FMPI Consultant:

Jiří Šilha, PhD.



General motivation

- **To describe the surface characteristic of unknown Space Debris object using BVRI photometric methods**
- **To classify objects according to the similarities in surface properties**
- **To investigate the influence of the space environment on the artificial materials**
- **To establish routines for data processing from BVRI photometry**

Space Debris

- All non-functional, human-made objects, which finished or lost its functionality
- Space debris research motivation:
 - To stabilize the population and avoid new fragmentation
 - Characterize existing objects, fragments and populations
 - Associate fragments with ancestors and assess the causes of their creation

Table: ESA space debris object classification. **Source:** ESA'S ANNUAL SPACE ENVIRONMENT REPORT

Type	Description	Type	Description
PL	Payload	RB	Rocket Body
PF	Payload Fragmentation Debris	RF	Rocket Fragmentation Debris
PD	Payload Debris	RD	Rocket Debris
PM	Payload Mission Related Object	RM	Rocket Mission Related Object

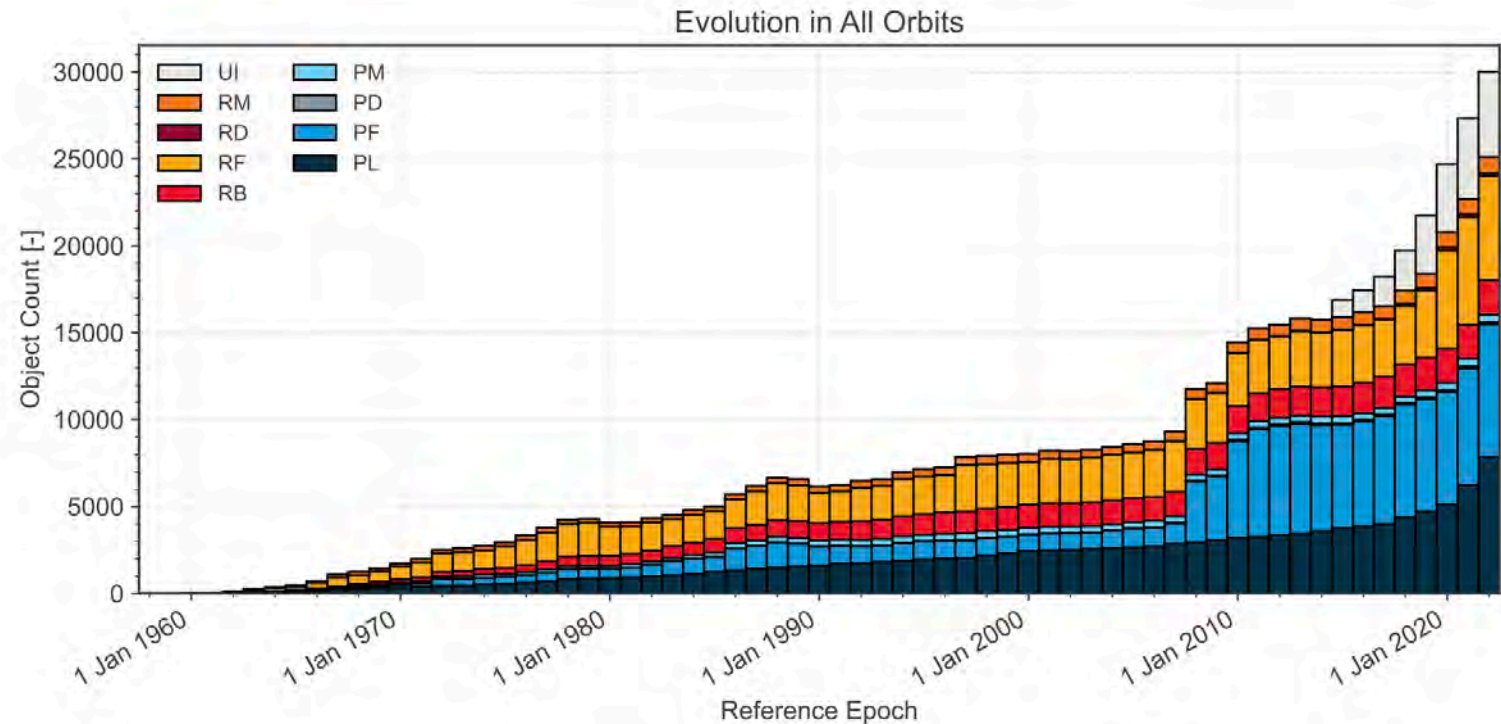


Figure: Evolution of number of objects in geocentric orbit by object class. **Source:** ESA'S ANNUAL SPACE ENVIRONMENT REPORT

Instrumentation

Sensor	AGO70
Mount	Equatorial (Open fork)
Tubes	1 Tube
Tube design	Newton
Diameter [m]	0.7
Focal length [mm]; ratio	2962.0; (f/4.2)
Camera	FLI Proline PL1001
CCD Chip	Kodak KAF-1001E
Dimension	24.5 x 24.5 mm 1024 x 1024
FOV	28.5 x 28.5 arc-min
iFOV [arc-sec/pix]	1.67

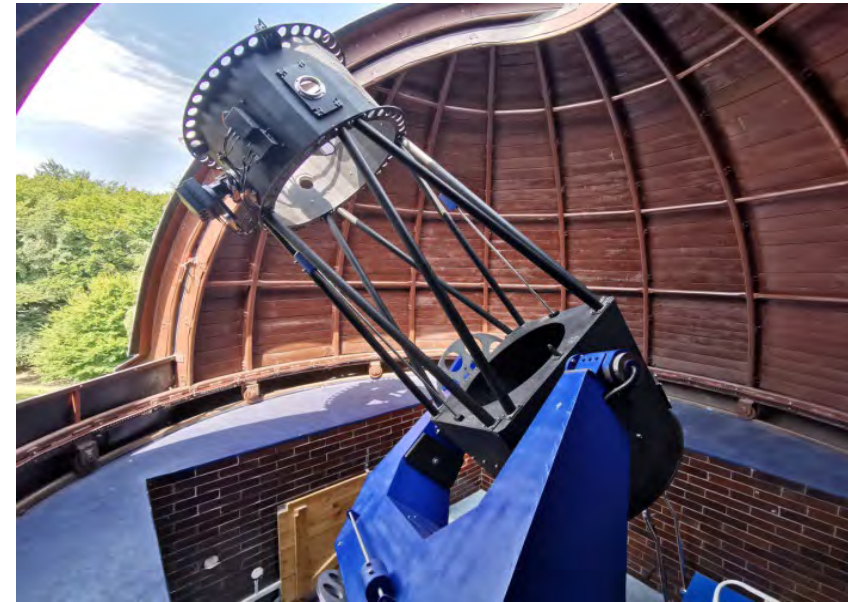


Figure: AGO70 in its Dome. Credit: Stanislav Griguš

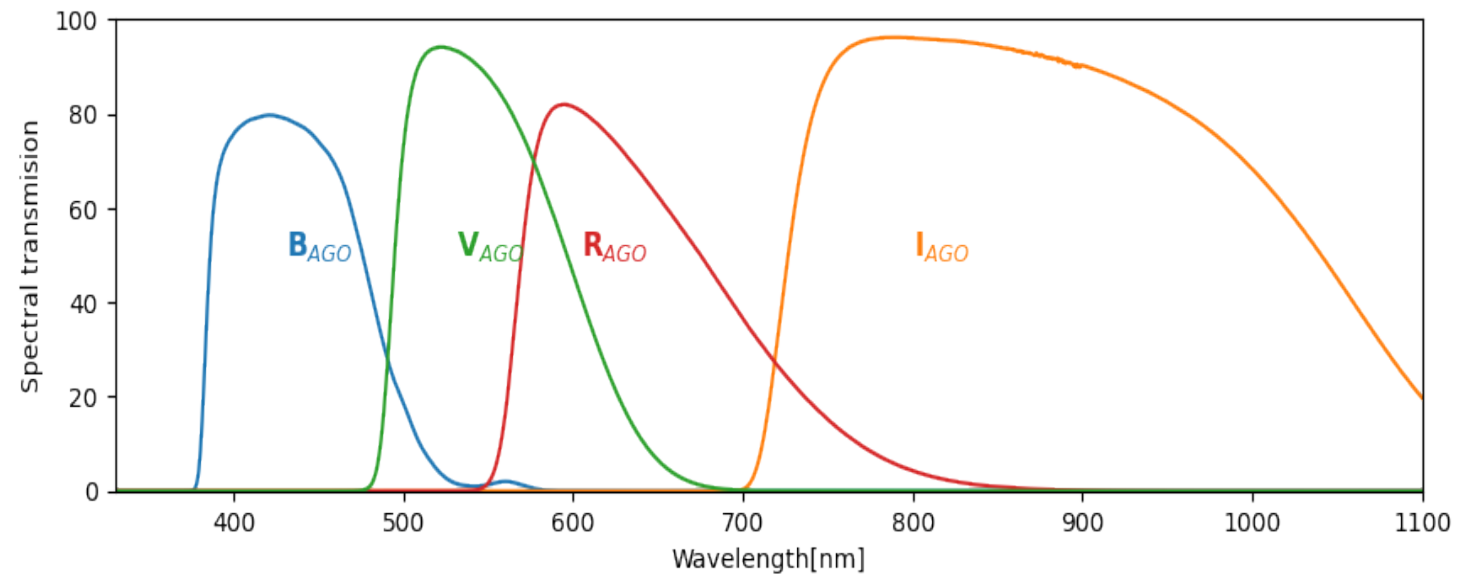


Figure: Photometric filters used at AGO70. Source: M.Bessel et al. 2004

BVRI Photometry

- Photometric method
 - Capturing of reflected Sunlight from target's surface
 - Surface properties are mapped into color indices
- Color index – numerical expression of target's color
 - Difference of magnitudes in two filters - B-V, R-I etc.
 - Depends on general geometry of observed passage
- Object characterization
 - Comparison of measured data with laboratory samples
 - Objects' classification according to the similarities in their reflections

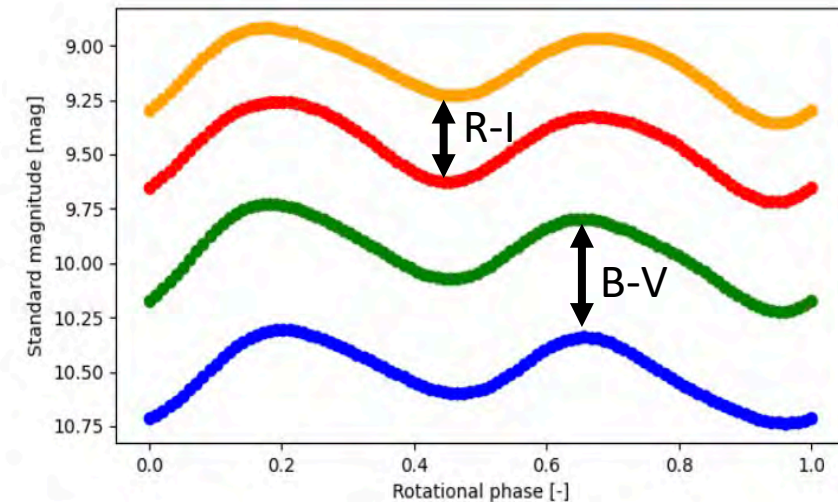


Figure: Demonstration of the color index meaning

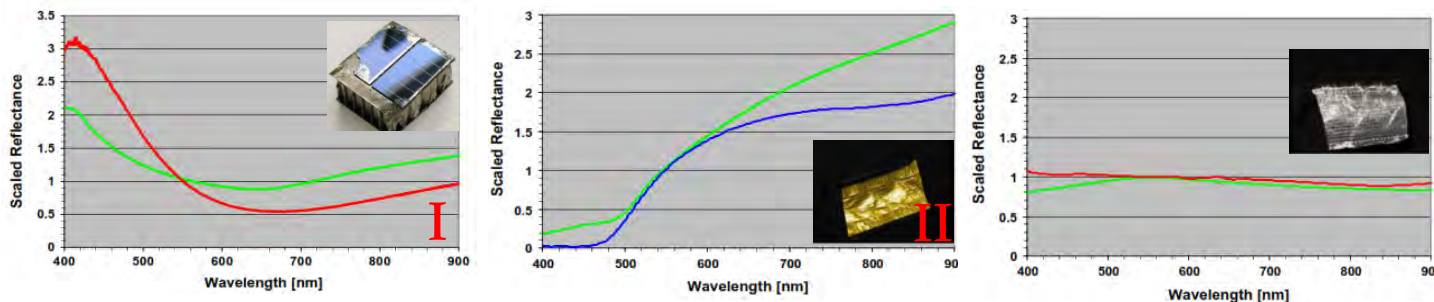


Figure: Representatives of the material groups with their spectra and material examples. Source: Vananti et al., 2017

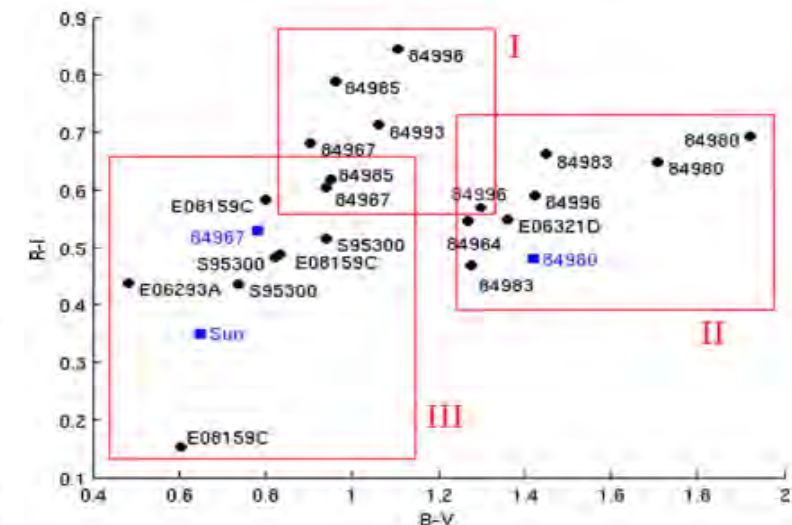


Figure: Material groups in the BVRI diagram. Source: Vananti et al., 2017

Photometric reduction

- Transformation into the standard system of magnitudes
- Landolt's catalog of standard stars (Landolt, 1992, 2009)
- Two-step linear optimization
- Extinction coefficient - k_f
 - Correction for the losses caused by atmosphere in specific airmass
 - Measure stars with **CI** close to zero
- Zero-point and color term - ZP_f, t_f
 - General scaling factor and color correction
 - Measure clusters of stars with different color indices and magnitudes

Transformation coefficients

$$M_f = m_f + ZP_f - k_f * X + t_f * (CI)$$

Figure: Transformation equation into the standard system of magnitudes

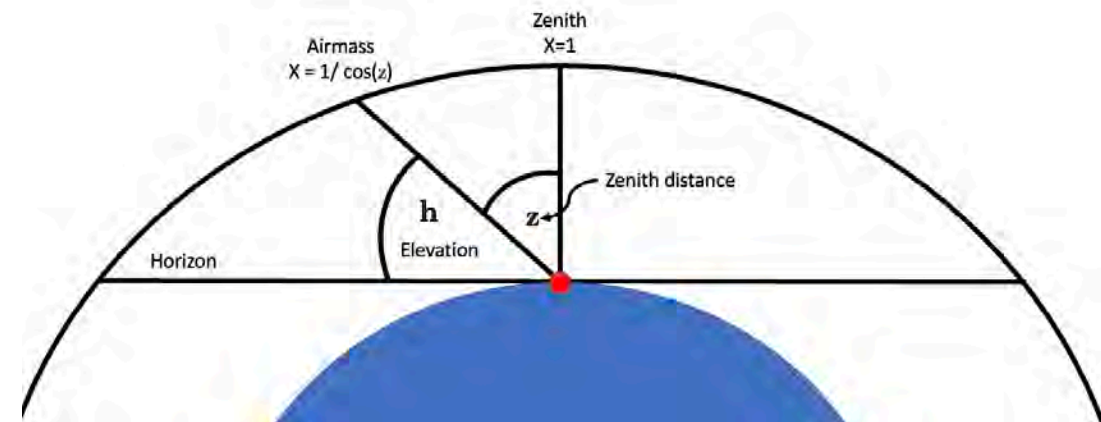


Figure: Airmass definition

Color indices

- Affected by number of effects
 - Phase angle and phase curve
 - Shape of target
 - Rotation state
 - Incident angle
 - Age of surface materials

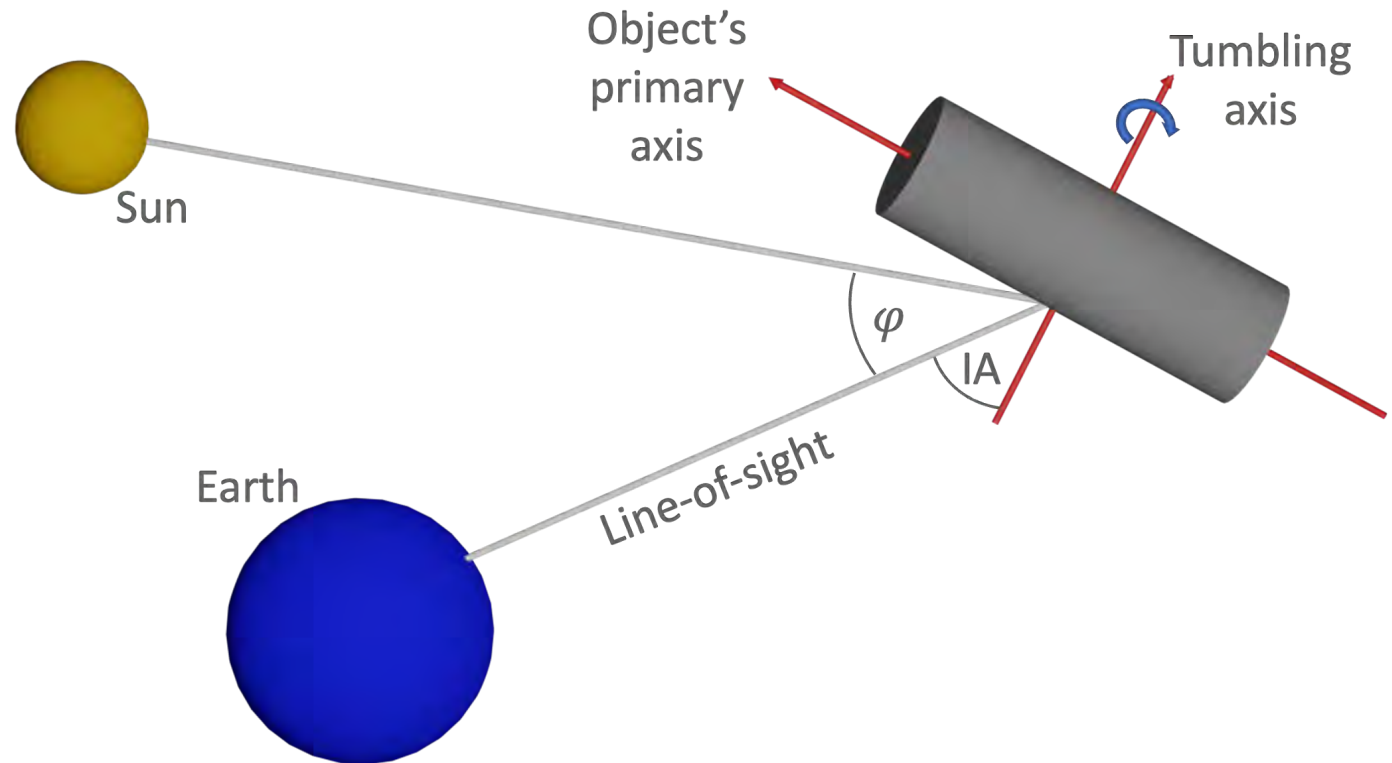


Figure: State vector and rotation axis angle i.e incident angle

Space-weathering and aging

- Characterization to:
 - Assess the material resistance against the environment
 - To fully understand the physics behind the space-weathering processes
- Change of the target's surface properties caused by the exposure to the space environments
 - Laboratory based measurements showed 'reddening'
 - Non-constant change of reflectivity - faster increase in the absorption in the lower wavelengths
 - Reddening - transmission received through the filter with the longer central wavelength being brighter than through the filter with the shorter central wavelength - *Engelhart et al., 2017*

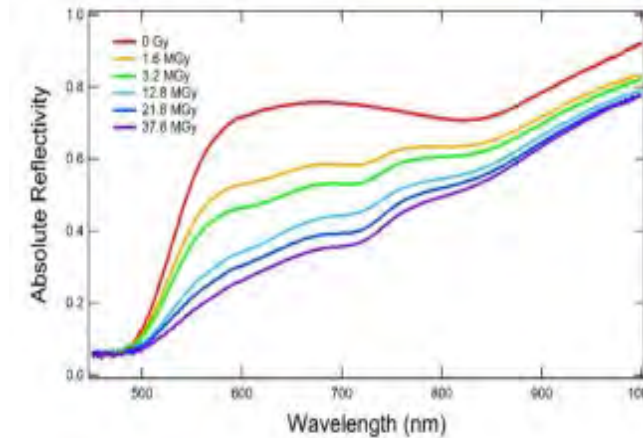


Figure: Change in the Absolute reflectivity of the measured samples after the different doses. **Source:** Engelhart et al., 2017

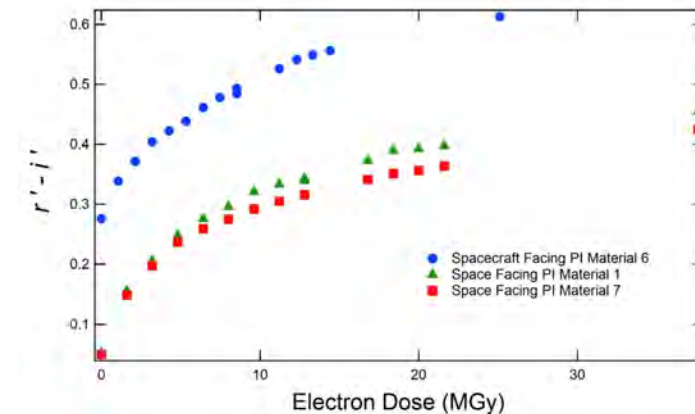


Figure: Change in the $r'-i'$ color index of three measured samples after the different doses. **Source:** Engelhart et al., 2017

Space-weathering and aging

- Change of the target's surface properties caused by the exposure to the space environments
 - Laboratory based measurements showed many common materials overgoes the 'reddening' (Engelhart, 2018)
 - Non-constant change of reflectivity - faster increase in the absorption in the lower wavelengths
 - White paint (commonly used on R/B coating) overgoes different changes – overall decrease of the reflectivity in the first years
 - Then non-constant reflectivity decrease wavelength dependent

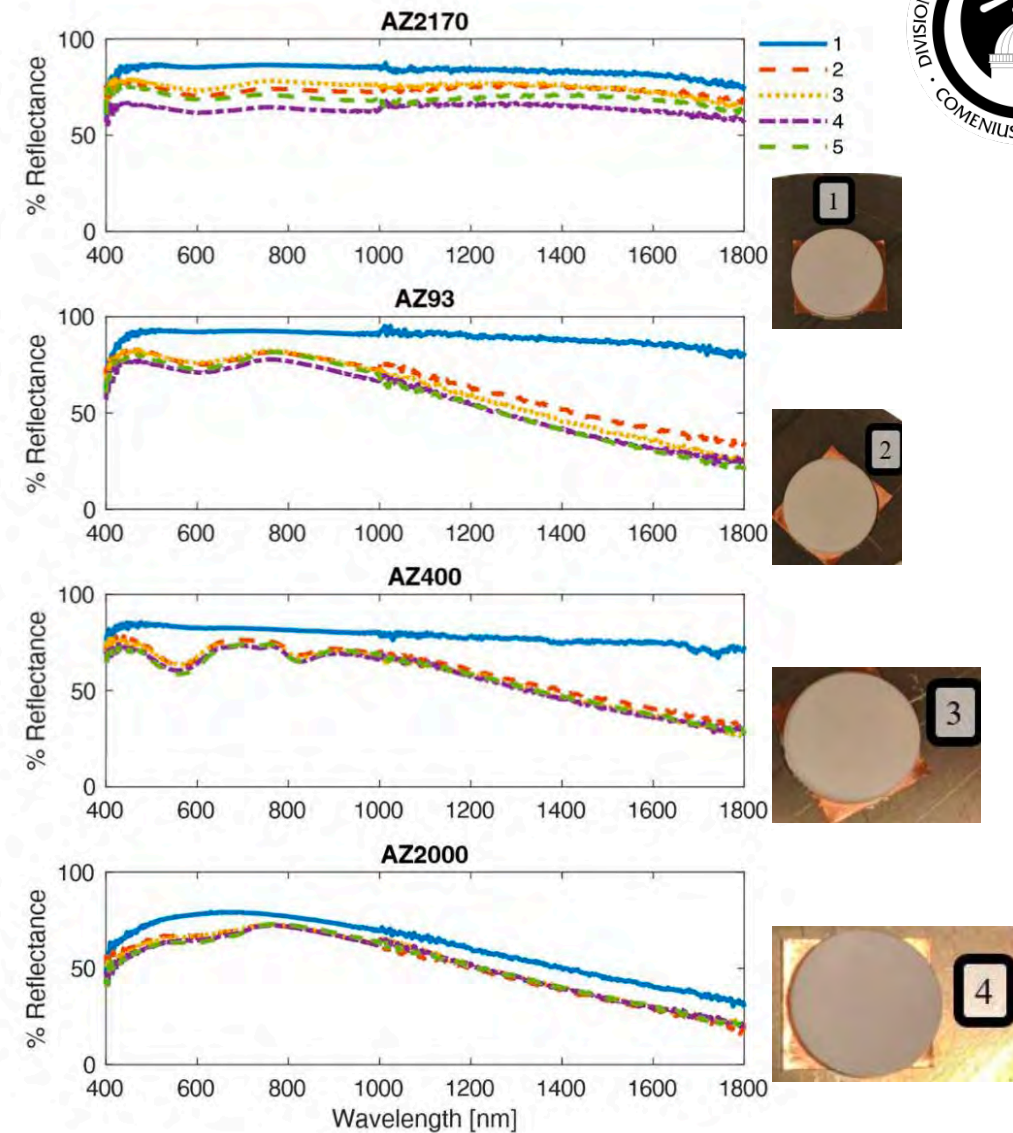


Figure: Changes in the Absolute reflectance of the measured samples after 5 different doses. **Source:** Hoffman et al., 2018

Space-weathering and aging

- Characterization to:
 - Assess the material resistance against the environment
 - To fully understand the physics behind the space-weathering processes
- Change of the target's surface properties caused by the exposure to the space environments
 - Observation based measurements showed 'blueing' - increase in the absorption in the lower wavelengths
 - Blueing – transmission through the filter with the shorter central wavelength being brighter than through the filter with the longer central wavelength - *Pearce et al., 2019*
- Two observational approaches:
 - Long term monitoring of the same object – AGO70 archive
 - Color index estimation for population of same bus types with different launch dates

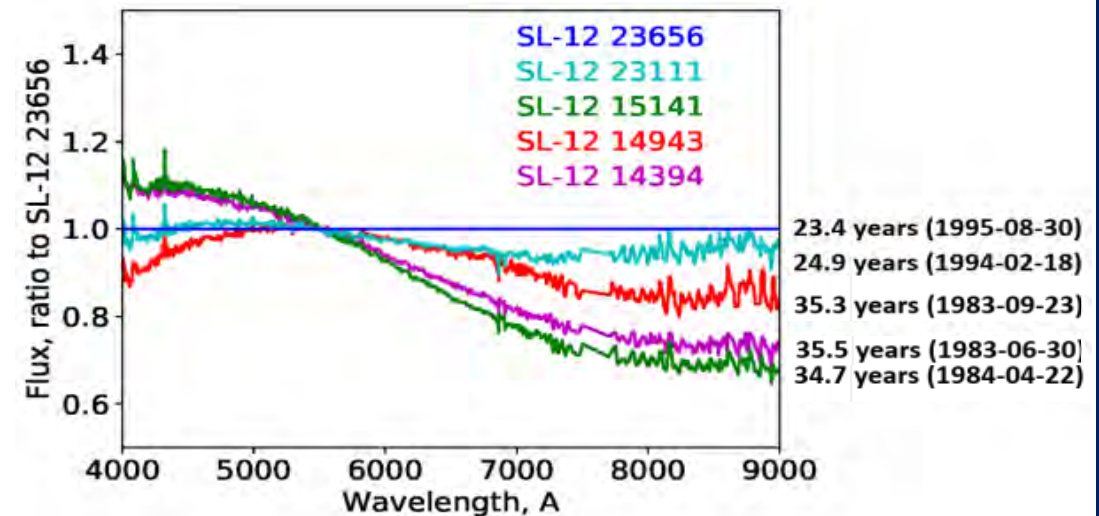


Figure: Reflective spectra of 5 SL-12 rocket bodies with different launch date, normalized by the youngest one. **Source:** Pearce et al., 2019

AGO70 observational campaign

- Long-term monitoring campaign since 2019
 - Geostationary functional satellites – attitude stabilized objects
 - Fast spinning cylindrical dual-spin satellites
 - Box-wing three-axis stabilized satellites
 - Geometry changes through the year due to the Earth's motion around the Sun
 - Varying distance influence the illumination state
 - Change of solar panels orientation
 - Affection by the Earth's shadow
 - Most stable geometrical conditions between vernal and autumnal equinoxes
 - To not introduce selection bias – use only the measurement from the same part of the year

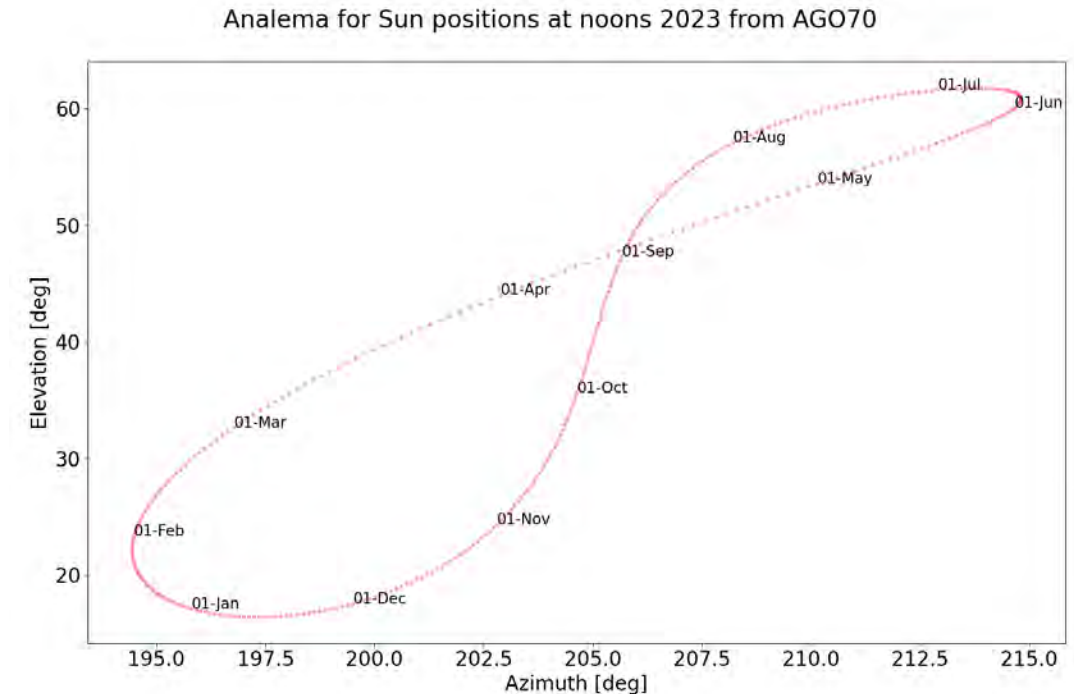


Figure: Sun positions at noon as seen from AGO70 during 2023

- Long-term monitoring campaign since 2019
 - Selected were 14 functional satellites along the GEO ring
 - Different architectures – Cube-wing satellites with different solar panels complexity or cylindrical bodies
 - Monthly monitoring
 - Each night at least 3 observations – before, near and after opposition – to minimize the phase angle effects
 - Each observation consist of number of exposures in all photometric passbands
 - All summer months are averaged to obtain annual color indices

Table: List of selected geostationary targets.

Name	COSPAR	NORAD	Lon [deg]	Origin	Shape
ABS 3A	2015-010A	40424	3.0 W	China	
THOR 7	2015-022A	40613	0.7 W	Norway	
MSG 4	2015-034A	40732	0.1 W	Germany	
SES 5	2012-036A	38652	5.0 E	Luxembourg	
EUTE 7B	2013-022A	39163	7.0 E	France	
COMSATBW-2	2010-021B	36582	13.2 E	Germany	
EUTE 16A	2011-057A	37836	15.9 E	France	
ASTRA 1N	2011-041A	37775	19.3 E	Luxembourg	
ASTRA 1L	2007-016A	31306	19.3 E	Luxembourg	
ASTRA 1KR	2006-012A	29055	19.3 E	Luxembourg	
ASTRA 1M	2008-057A	33436	19.3 E	Luxembourg	
EUTE 21B	2012-062B	38992	21.6 E	France	
EXPRESS	2015-082A	41191	36.1 E	Russia	
IRNSS 1F	2016-015A	41384	32.7 E	India	

- Long-term monitoring campaign since 2019
 - Selected were 14 functional satellites along the GEO ring
 - Different architectures – Cube-wing satellites with different solar panels complexity or cylindrical bodies
 - Monthly monitoring
 - Each night at least 3 observations – before, near and after opposition – to minimize the phase angle effects
 - Each observation consist of number of exposures in all photometric passbands
 - All summer months are averaged to obtain annual color indices

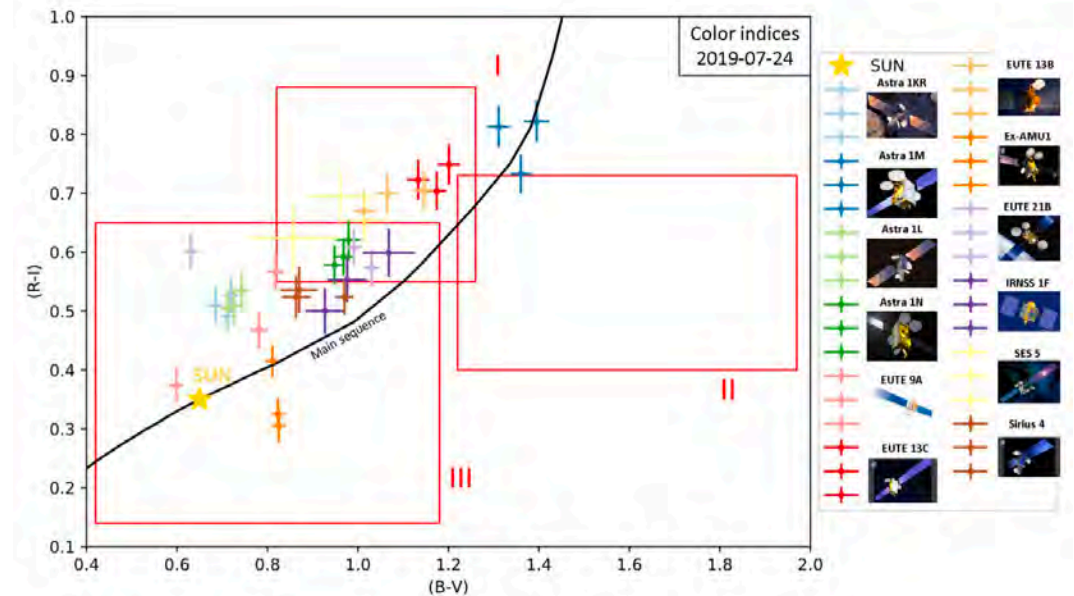
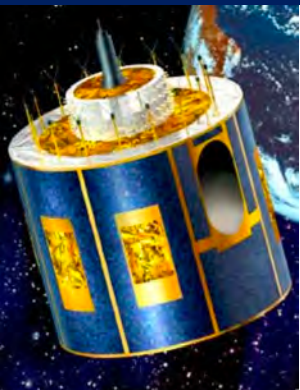
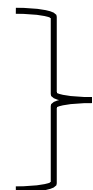


Figure: Snapshot of the color indices of all campaign GEO targets from the 24th of July, 2019. For each object presented are measurement under three different phase angles with their mean uncertainties.

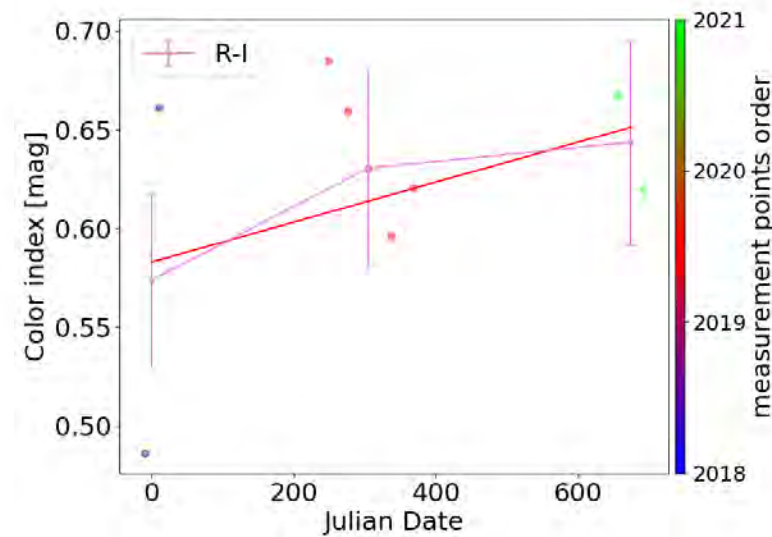
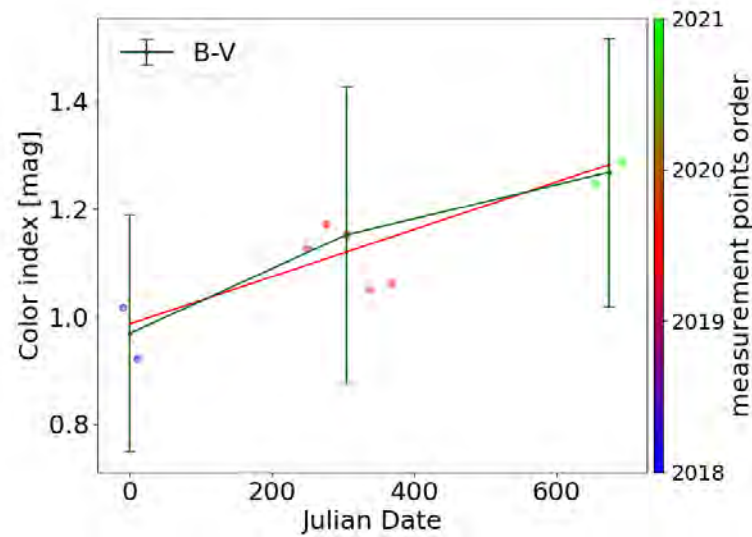
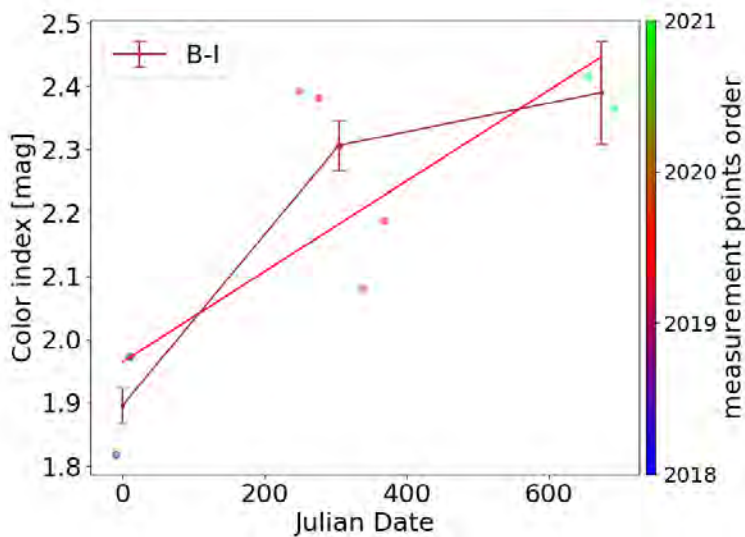
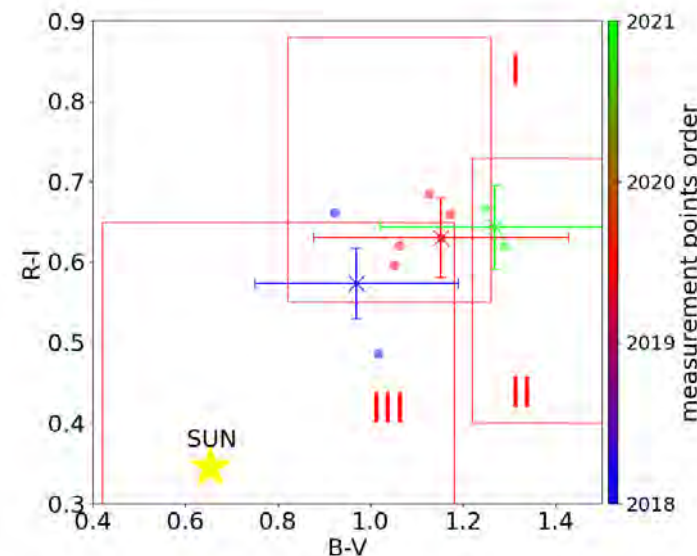


METEOSAT 11 (Cospas 2015-34A; Norad 40732)

- EUMETSAT – meteorological dual-spin GEO satellite
- Operational since 2015 – after fast weathering
- Annual color index changes rates
 - $\Delta(B-V) \sim 0.2$ mag
 - $\Delta(R_c I_c) \sim 0.05$ mag
 - $\Delta(B-I_c) \sim 0.25$ mag

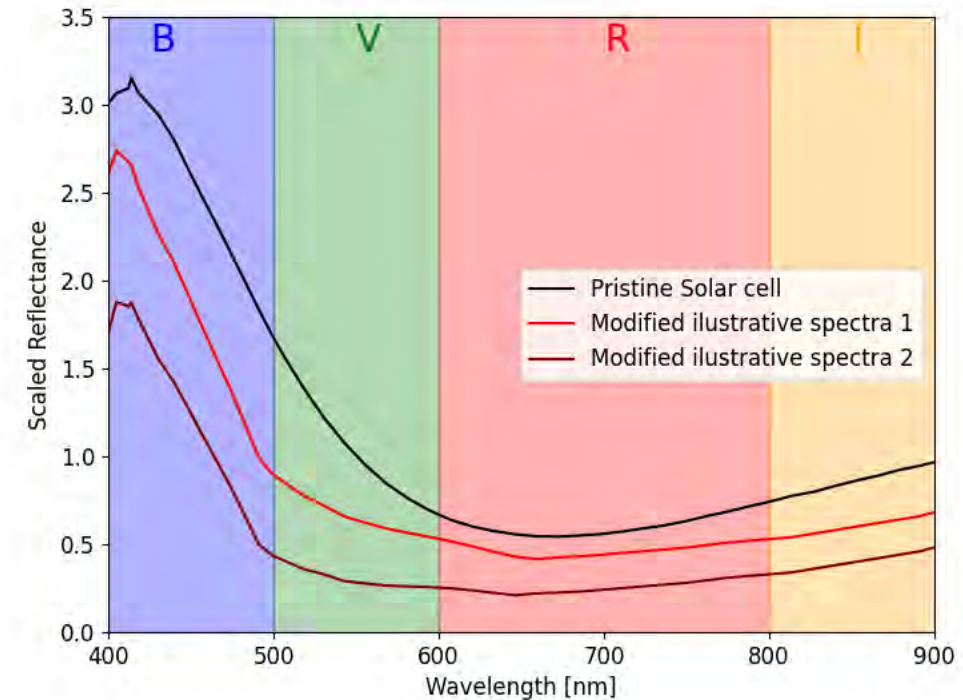


Reddening – Faster increase in (B-V) than in ($R_c I_c$)



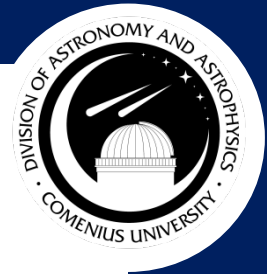
Conclusion

- Presented were:
 - Motivation and general aims of the PhD thesis
 - BVRI photometry basic idea for object characterization
 - GEO satellite long term monitoring campaign
 - Space weathering investigated on METEOSAT 11
- All routines developed are prepared to be run AGO70 data with different filter sets
 - Full pipeline for the photometric reduction
 - Python library of functions for the color light curve processing
- What next:
 - To continue with the monitoring of the GEO satellites
 - To automatized the data processing (after 4 years ~170 000 frames)
 - Process all measured satellites and estimate the space weathering and aging rates





Thank you for attention !



References

- ESA FAQ: https://www.esa.int/Safety_Security/Space_Debris/FAQ_Frequently_asked_questions
- ODQN 23i1 (2020) source: <https://orbitaldebris.jsc.nasa.gov/quarterly-news/pdfs/odqnv23i1.pdf>
- Gunter's Space Page (2020): https://space.skyrocket.de/doc_sdat/raduga.htm
- ŠILHA, Jiří, et al. Space debris observations with the Slovak AGO70 telescope: Astrometry and light curves. *Advances in Space Research*, 2020.
- Landolt, Arlo U. UBVRI photometric standard stars in the magnitude range 11.5-16.0 around the celestial equator. *Astronomical Journal* (ISSN 0004-6256), vol. 104, no. 1, July 1992, p. 340-371, 436-491
- Vananti, A., Schildknecht, T., & Krag, H. (2017). Reflectance spectroscopy characterization of space debris. *Advances in Space Research*, 59(10), 2488-2500. doi:10.1016/j.asr.2017.02.033
- HAMARA, M.; Rotation properties of the artificial objects in the vicinity of Earth; Dissertation Thesis; Comenius University in Bratislava; Faculty of Mathematics, Physics and Informatics Bratislava 2017, Retrieved from <http://opac.crzp.sk/?fn=detailBiblioForm&sid=F065241B7212E93A23176233722A&seo=CRZP-detail-kniha> [Date of access: 2020-11-10]
- COWARDIN, H.M.: CHARACTERIZATION OF ORBITAL DEBRIS OBJECTS OVER OPTICAL WAVELENGTHS VIA LABORATORY MEASUREMENTS; Dissertation Thesis; University of Houston; the Faculty of the Department of Physics Houston May 2010
- FEIGELSON, E. D.; BABU, G. J. 2012. *Modern Statistical Methods for Astronomy*. Cambridge University Press. ISBN: 978-0-521-76727-9, s. 292 - 36
- Engelhart, D. P., et al. "Space weathering experiments on spacecraft materials." *The Journal of the Astronautical Sciences* 66.2 (2019): 210-223.
- Cordelli, Emiliano, Peter Schlatter, and Thomas Schildknecht. "Simultaneous multi-filter photometric characterization of space debris at the Swiss Optical Ground Station and Geodynamics Observatory Zimmerwald." *Advanced Maui Optical and Space Surveillance Technologies Conference (AMOS)*. 2018.
- SCHILDKNECHT, Thomas, et al. Reflectance spectra of space debris in GEO. In: *Proceedings of the 2009 AMOS Technical Conference*. Maui Economic Development Board Inc Kihei, Maui, HI, 2009.
- BUZZONI, Alberto, et al. Toward a Physical Characterization of the Soviet/Russian Constellation of Molniya Satellites. *LPICo*, 2019, 2109: 6067.
- Šilha et al., AGO70: passive optical system to support SLR tracking of space debris on LEO, *Proceedings of AMOS Conference*, Maui, Hawaii, 2021.